Picosecond Coherent Optical Manipulation of a Single Electron Spin in a Quantum Dot

J. Berezovsky, *et al.*

Science **320**, 349 (2008);
DOI: 10.1126/science.1154798

Science (print ISSN 0036-8075; online ISSN 1095-9203) is published weekly, except the last week in December, by the American Association for the Advancement of Science, 1200 New York Avenue NW, Washington, DC 20005.

Picosecond Coherent Optical Manipulation of a Single Electron Spin in a Quantum Dot

J. Berezovsky,* M. H. Mikkelsen,* N. G. Stoltz, L. A. Coldren, D. D. Awschalom†

Most schemes for quantum information processing require fast single-qubit operations. For spin-based qubits, this involves performing arbitrary coherent rotations of the spin state on time scales much faster than the spin coherence time. By applying off-resonant, picosecond-scale optical pulses, we demonstrated the coherent rotation of a single electron spin through arbitrary angles up to π radians. We directly observed this spin manipulation using time-resolved Kerr rotation spectroscopy and found that the results are well described by a model that includes the electron-nuclear spin interaction. Measurements of the spin rotation as a function of laser detuning and intensity confirmed that the optical Stark effect is the operative mechanism.

Using ultrafast optical pulses to coherently manipulate the spin state of an electron is a key ingredient in many proposals for solid-state quantum information processing (*1*–*6*). Although electrical control of a single spin has been achieved (*7*, *8*), the nanosecond time scales required for such manipulation limit the number of operations that can be performed within the spin coherence time. In contrast, spin control via picosecond-scale optical pulses yields an improvement of several orders of magnitude in the manipulation time, as required for many proposed applications. Additionally, this all-optical technique provides simple pathways for coupling the quantum degrees of freedom of a single spin and a photon—a useful property for enabling quantum communication. We experimentally demonstrated such a scheme for a single electron spin in a quantum dot (QD).

The optical (or ac) Stark effect (OSE) was first studied in atomic systems in the 1970s (*9*–*11*) and was subsequently explored in bulk semiconductors and quantum wells (*12*–*14*). In recent years, the OSE has been used to observe ensemble spin manipulation in a quantum well (*15*) and to control orbital coherence in a QD (*16*). Additionally, other optical manipulation schemes have been explored (*17*–*20*), which, in contrast to this work, affect the average polarization of a spin ensemble instead of directly manipulating individual spin states. Using perturbation theory, it is found that an optical field with intensity I_{tip}, detuned from an electronic transition by an energy Δ, induces a shift in the transition energy

$$\Delta E \approx \frac{D^2 I_{tip}}{\Delta\sqrt{\varepsilon/\mu}} \qquad (1)$$

where D is the dipole moment of the transition, and ε and μ are the permittivity and permeability of the material (*13*). In the relevant energy levels for the QD system considered here (Fig. 1B), the ground state consists of a single electron in the lowest conduction band level, spin-split by a small magnetic field B_z. The lowest-energy interband transition is to the trion state, consisting of two electrons in a singlet state and a heavy hole. Because of the optical selection rules, the dipole strength of this transition in the basis along the $\hat{y}$ direction from the spin-up ground state is zero for σ^+ polarized light and from the spin-down ground state is zero for σ^- polarized light, as indicated in the diagram. Therefore, for circularly polarized light, the OSE shifts just one of the spin sublevels and produces a spin splitting in the ground state that can be represented as an effective magnetic field, B_{Stark}, along the light-propagation direction. By using ultrafast laser pulses with high instantaneous intensity to provide the Stark shift, large splittings can be obtained to perform coherent manipulation of the spin within the duration of the optical pulse (here, B_{Stark} ~ 10 T). This phenomenon can also be described in terms of a stimulated Raman transition (*3*, *6*, *20*).

The sample we used consisted of a layer of charge-tunable gallium arsenide (GaAs) interface QDs embedded in an optical cavity. [Details of the sample structure and characterization are given in (*21*–*23*).] In the experimental setup (Fig. 1C), three synchronized, independently tunable optical pulse trains are focused onto the sample: the pump, the probe, and the tipping pulse (TP). The pump and tipping pulse are both derived from a mode-locked Ti:sapphire laser generating a train of ~150-fs pulses at a repetition rate of 76 MHz. The pump is circularly polarized and tuned to an energy E = 1.646 eV [full width at half maximum (FWHM) ~ 1 meV], thereby injecting spin-polarized electrons and holes into the continuum of states above the QD (*24*). One or more of these electrons or holes can then relax into the QD. The circularly polarized TP (duration ~ 30 ps, FWHM = 0.2 meV) is tuned to an energy below the lowest QD transition (Fig. 1A) and is used to induce the Stark shift. The relative time delay between the pump pulse and the TP is controlled by a mechanical delay line in the pump path.

The probe pulse is generated by passing a narrow-linewidth continuous-wave laser through an electro-optic modulator synchronized with the pump/TP laser. The resulting 1.5-ns pulses probe the spin in the QD through the magneto-optical Kerr effect (*23*). This effect arises from the real part of the dielectric response function of the QD and results in a spin-dependent rotation of the polarization of the linearly polarized probe upon reflection off of the sample. As the energy of this probe light is scanned across the QD transi-

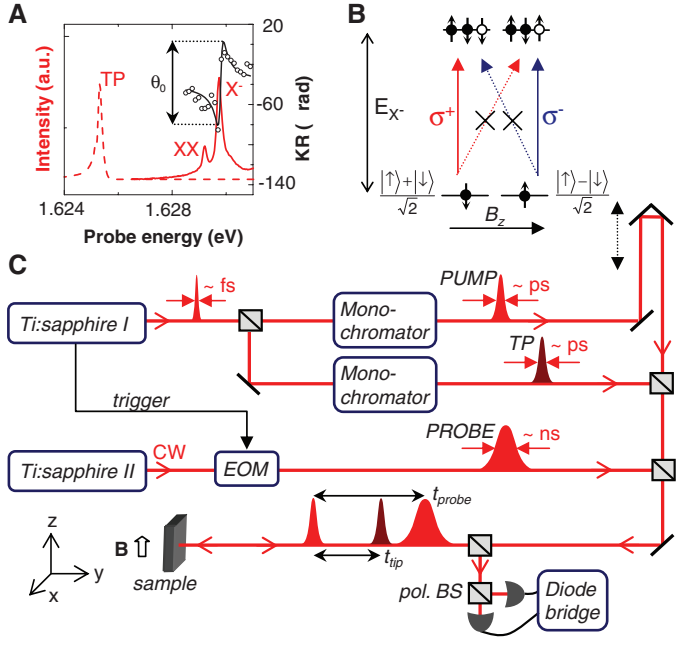

Fig. 1. (**A**) The solid red line shows trion (X^-) and biexciton (XX) photoluminescence from a single QD. The black data points show the corresponding single-spin KR, and the black line is an odd-Lorentzian fit to this data, from which the KR amplitude θ_0 is obtained. The dashed line shows the TP spectrum at a detuning of 4.4 meV. a.u., arbitrary units. (**B**) Diagram of the singly charged QD ground state and the optically allowed transitions to the trion state. The solid circles represent electrons and the open circles represent heavy holes. (**C**) Schematic of the experimental setup. CW, continuous wave; EOM, electro-optic modulator; pol. BS, polarizing beamsplitter.

Center for Spintronics and Quantum Computation, University of California, Santa Barbara, CA 93106, USA.

*These authors contributed equally to this work.
†To whom correspondence should be addressed. E-mail: awsch@physics.ucsb.edu

tion energy, E_{X^-}, an odd-Lorentzian line shape $[\propto x/(1+x^2)]$ centered at the transition energy is seen in the Kerr rotation (KR) spectrum (*22*, *25*). By fitting such a curve (as shown in Fig. 1A), we can extract the amplitude of this feature, θ_0, which is proportional to the projection of the spin polarization in the QD along the light-propagation direction.

In a typical measurement, the pump pulse arrives at time (t) = 0 along the y axis (growth direction), and in some cases, a single spin-polarized electron will relax into the QD. For pump helicity $\sigma^{\pm}$, this electron is (up to a global phase) initially in the state $\psi(t=0) = (|\uparrow\rangle \pm i|\downarrow\rangle)/\sqrt{2}$, where "up" and "down" are chosen as the basis along the external magnetic field B_z. The spin then begins to coherently precess at the Larmor frequency $\omega = g\mu_B B_z/\hbar$: $\psi(t) = (\exp(-i\omega t/2)|\uparrow\rangle \pm i\exp(i\omega t/2)|\downarrow\rangle)/\sqrt{2}$, where g is the effective electron g factor, μ_B is the Bohr magneton, and $\hbar$ is the reduced Planck constant. At $t = t_{tip}$, the TP arrives and generates an additional spin splitting along the y axis for the duration of the pulse. During this time, the spin precesses about the total effective field (which is typically dominated by B_{Stark}) and then continues to precess about the static applied field. The probe then measures the resulting projection of the spin in the QD, $\langle S_y \rangle$ at $t = t_{probe}$. This sequence is repeated at the repetition frequency of the laser (76 MHz), and the signal is averaged for several seconds for noise reduction. The pump and probe are modulated with mechanical choppers, allowing for lock-in detection to measure only spins that are injected by the pump. Furthermore, the pump is switched between σ^+ and σ^-, with a measurement made at each helicity. The spin signal is then taken as the difference between these values, eliminating any spurious signal from spins not generated by the pump [such as phonon-assisted absorption from the TP (*26*)].

To map out the coherent dynamics of the spin in the QD, KR spectra are measured as a function of pump-probe delay. Figure 2A shows a plot of the KR angle, θ_K as a function of probe energy and t_{probe} with an applied field B_z = 715 G and no TP. Horizontal line cuts display the dispersive line shape centered at the transition energy E_{X^-} (as shown in Fig. 1A). As t_{probe} is swept along the vertical axis, the precession of the spin can be seen as the oscillations in θ_K. When the TP is applied at t_{tip} = 1.3 ns, as in Fig. 2B, there is a substantial change in the KR spectra. For $t < t_{tip}$, the KR signal is essentially the same as in Fig. 2A, but for $t > t_{tip}$ the sign of the signal is reversed. This can be clearly seen in the line cuts in Fig. 2, C to F. Line cuts in (C) and (D) are both before the TP and show the same behavior, whereas the line cut in (F) has the opposite sign of the line cut in (E) as a result of the TP.

It is convenient to understand the observed spin dynamics in the Bloch sphere picture. Here, the spin state is represented as a vector (S_x, S_y, S_z), where $(0, 0, \pm S_z)$ represents the eigenstates $|\uparrow\rangle$ and $|\downarrow\rangle$, and vectors with nonzero S_x and S_y represent coherent superpositions of $|\uparrow\rangle$ and $|\downarrow\rangle$. In this picture, the dynamics of the spin can be calculated by applying the appropriate sequence of rotation matrices to the initial state (*21*). The effect of the pump and the TP thus results in the spin state as a function of time

$$\vec{S}(t) = \begin{cases} \begin{pmatrix} S_{0,y}\sin\omega t \\ S_{0,y}\cos\omega t \\ S_{0,z} \end{pmatrix} & 0 < t < t_{tip} \\ \begin{pmatrix} S_{0,y}(\cos\phi_{tip}\sin\omega t_{tip}\cos\omega t' + \\ \cos\omega t_{tip}\sin\omega t') - \\ S_{0,z}\sin\phi_{tip}\cos\omega t' \\ S_{0,y}(-\cos\phi_{tip}\sin\omega t_{tip}\sin\omega t' + \\ \cos\omega t_{tip}\cos\omega t') - \\ S_{0,z}\sin\phi_{tip}\sin\omega t' \\ S_{0,y}\sin\phi_{tip}\sin\omega t_{tip} + S_{0,z}\cos\phi_{tip} \end{pmatrix} & t \geq t_{tip} \end{cases} \quad (2)$$

where the initial spin state is $(0, S_{0,y}, S_{0,z})$, $t' = t - t_{tip}$, ω is the precession frequency about the z axis, and ϕ_{tip} is the angle through which the spin precesses during the TP. Here we have included an initial component of the spin along the z axis to account for small misalignments of the pump beam. Because the duration of the TP is much less than ω^{-1}, the tipping is assumed to occur instantaneously.

As can be seen from Eq. 2, the TP may result in a substantial nonprecessing component of the spin along the z axis. Through the hyperfine interaction, electron spins can flip with nuclear spins. The component of the nuclear spin along the external field B_z does not precess and therefore can build over time in the process of dynamic nuclear polarization (DNP) (*24*, *27*). As nuclear polarization builds along the z axis, it acts back on the electron spin as an effective magnetic field $B_n\hat{z}$. Thus in Eq. 2, ω must be replaced by $\omega' = \omega + \omega_n$. ω_n ($= g\mu_B B_n/\hbar$) is proportional to the steady-state nuclear polarization, which in turn is proportional to S_z. Thus, equating ω_n and S_z with a constant of proportionality α, we have $\omega_n = \alpha(S_{0,y}\sin\phi_{tip}\sin(\omega+\omega_n)t_{tip} + S_{0,z}\cos\phi_{tip})$.

Solving this equation numerically for ω_n and substituting ω' into Eq. 2 self-consistently yield the coherent spin dynamics of the system as a function of time. To model the results below, we include the finite spin coherence time, T_2^*, and a phenomenological I_{tip}-dependent term to account for imperfect fidelity of the spin rotations or other background effects, with a characteristic scale I_0. The decoherence term is taken as exponential, in agreement with previous measurements on this sample (*23*). Finally, we take the difference between σ^+ and σ^- pump helicity, yielding

$$\theta_0(t;\vec{S}_0,\omega,I_{tip},\alpha,T_2^*,I_0) = [S_y(t;\vec{S}_0) - S_y(t;-\vec{S}_0)]\exp(-t/T_2^*)\exp(-I_{tip}/I_0) \quad (3)$$

Figure 3A shows the time evolution of a single spin in a transverse magnetic field, with no TP applied. Each data point is determined from the fit to a KR spectrum at a given pump-probe delay, as in Fig. 2. If we convolve Eq. 3 with the measured profile of the probe pulse, we can perform a least-squares fit to this data and determine various parameters in the model: ω, T_2^*, and the effective field from the nuclear polarization, B_n. The red curve in Fig. 3A shows the result of this fit, yielding ω = 1.39 GHz, T_2^* = 5.5 ns, and B_n = 68 G, and the dotted line is the corresponding plot of Eq. 3 without the probe pulse convolution. As expected, the spin is initialized at t = 0 and then precesses freely about the applied field.

The data in Fig. 3, B and C, show the same coherent spin dynamics as those in Fig. 3A, but with the TP applied at $t = t_{tip}$. The intensity of the TP is chosen to induce a 1.05 × π rotation about the y axis, which is determined as discussed below. In Fig. 3B, the TP arrives at t_{tip} = 1.3 ns, when the projection of the spin is mainly along the x axis. This component of the spin is thus rotated by the TP through ~π radians. The

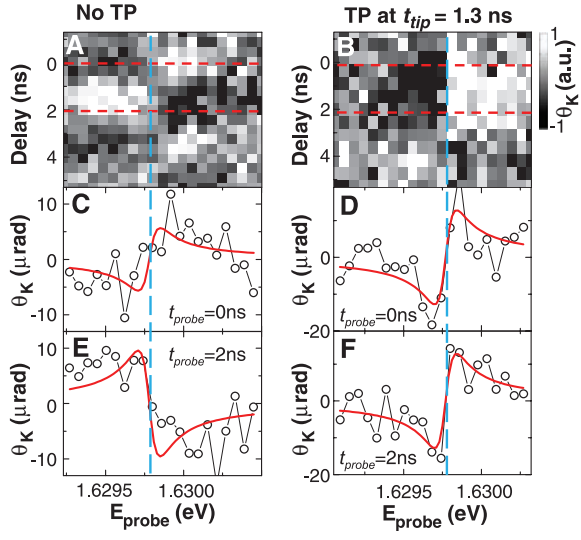

Fig. 2. (**A** and **B**) KR as a function of probe energy and pump-probe delay. White represents positive KR, black represents negative KR, and the dashed blue line indicates the transition energy E_{X^-}. (A) shows spin precession in the absence of the TP; in (B), the TP is applied at t_{tip} = 1.3 ns, with $I_{tip} = 4.7 \times 10^5$ W/cm^2 and Δ = 2.65 meV. A constant offset is subtracted from each KR spectrum. (**C** to **F**) Line cuts (black curves with data points) taken along the dashed red lines in (A) and (B) showing the effect of the TP. (C) and (E) are with no TP and t_{probe} = 0 and 2 ns, respectively; in (D) and (F), t_{tip} = 1.3 ns and t_{probe} = 0 and 2 ns, respectively. The solid red curves are odd-Lorentzian fits from which the KR amplitude θ_0 is extracted.

predicted spin dynamics as given by Eq. 3 is shown in the dotted red line, and the same curve convolved with the probe pulse is given by the solid red line. This curve is not a fit: All of the parameters are determined either in the fit to Fig. 3A or as discussed below. Only the overall amplitude of the curve has been normalized. Here, the spin is initialized at $t = 0$, and as before, precesses freely until the arrival of the TP. After the TP, the spin has been flipped and the resulting coherent dynamics show a reversal in sign. This can be clearly seen by comparing the sign of the measured signal at the position indicated by the dashed line in Fig. 3.

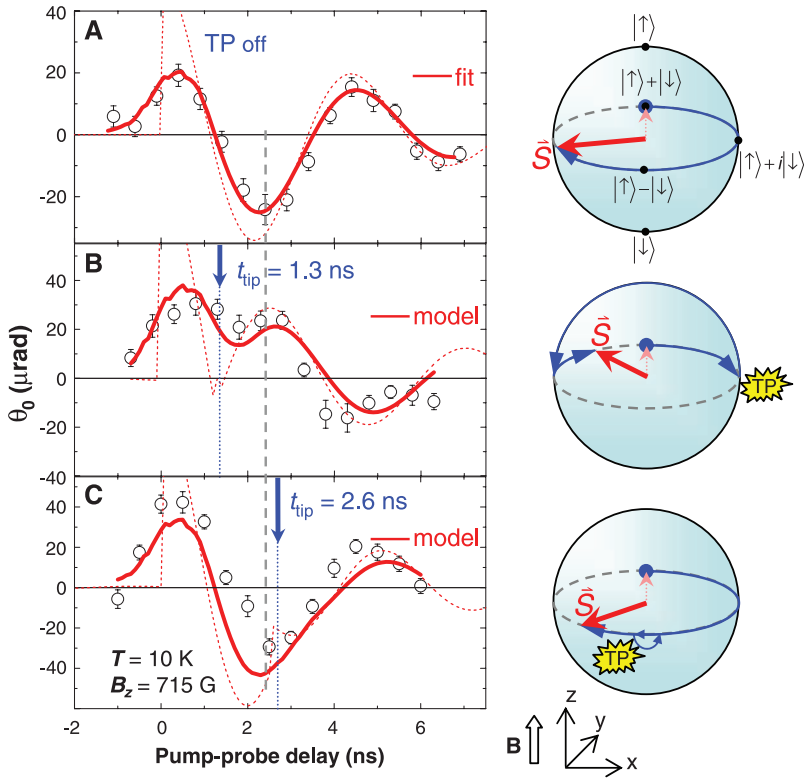

Fig. 3. (A) Coherent single-spin precession in a transverse magnetic field (B_z = 715 G), with error bars determined as the standard error from the fits to the KR spectra. The solid red line is a fit to Eq. 3 convolved with the probe pulse, and the dotted red line line shows Eq. 3 without the probe pulse convolution. The diagrams on the right schematically show the evolution of the spin on the Bloch sphere. (**B** and **C**) Spin dynamics under the same conditions as in (A), but with the TP applied at t_{tip} = 1.3 ns (B) and 2.6 ns (C) to induce a 1.05 × π rotation about $\hat{y}$, with the TP detuning Δ = 2.65 meV and intensity I_{tip} = 4.7 × 10^5 W/cm^2. The solid red lines show model curves of Eq. 3 using parameters obtained elsewhere, with probe pulse convolution; the dotted red lines show model curves without probe pulse convolution.

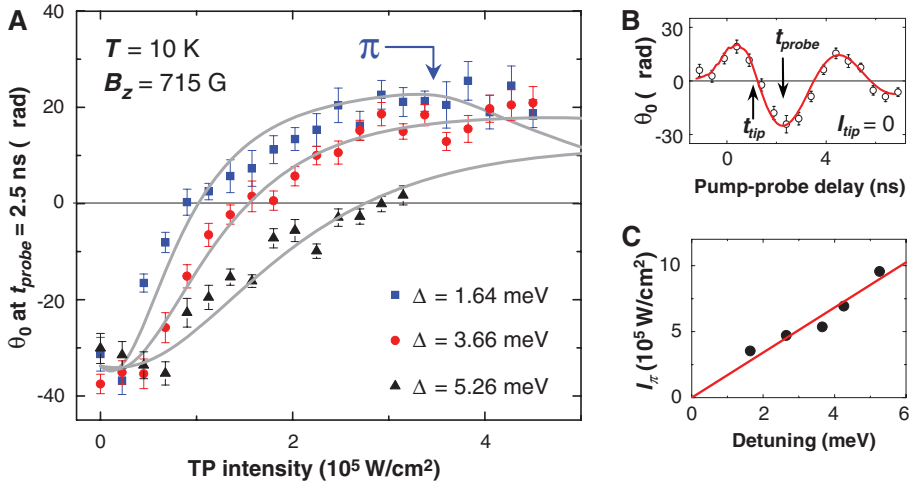

Fig. 4. (**A**) Single-spin KR amplitude θ_0 as a function of TP intensity, at three detunings from the X$^-$ transition. The TP arrives at t_{tip} = 1.3 ns, and the probe is fixed at t_{probe} = 2.5 ns, as illustrated in (**B**). The gray lines are fits to Eq. 3, varying only a single parameter, the strength of the OSE (β), and using the parameters from the fit to Fig. 2A, $S_{0,z}/S_{0,y}$ = −0.11 and I_0 = 6.9 × 10^5 W/cm^2. The TP intensity, I_π, required for a π rotation at Δ = 1.64 meV is indicated by the arrow. (**C**) I_π as a function of Δ, as obtained from the fits.

Figure 3C shows the spin dynamics again with the same parameters, but with t_{tip} = 2.6 ns. The spin at this delay will have only a small projection in the *x*-*z* plane, and the TP-induced rotation about the *y* axis will have only a small effect on the spin state. This expectation is borne out in the data, where the spin dynamics show essentially the same behavior as in the absence of the TP (Fig. 3A). Again, the model yields qualitatively the same behavior.

Further details of this spin manipulation can be investigated by varying the TP intensity I_{tip} and the detuning Δ of the TP from the QD transition energy for a fixed t_{probe} and t_{tip} (Fig. 4B). In Fig. 4A, the KR signal θ_0 as a function of I_{tip} is shown at t_{probe} = 2.5 ns, with the TP arriving at t_{tip} = 1.3 ns, for three different values of Δ. When I_{tip} = 0, the spin precesses undisturbed and yields a negative signal at t_{probe} = 2.5 ns (as in Fig. 3A). As I_{tip} is increased, the spin is coherently rotated through an increasingly large angle, and the observed signal at t_{probe} = 2.5 ns changes sign and becomes positive (as in Fig. 3B). Furthermore, the strength of the OSE is expected to decrease linearly with the detuning Δ (Eq. 1). The gray lines in Fig. 4A are plots of Eq. 3 with parameters taken from the fit in Fig. 3A, and $\phi_{tip} = \beta I_{tip}$. From these curves, we additionally obtain the phenomenological factor I_0 = 6.9 × 10^5 W/cm^2. This same value is used in all of the model curves shown. From this, we can estimate the fidelity of a π rotation to be approximately 80% (*21*). The only parameter that is changed between the three curves in Fig. 4A is the strength of the OSE, β. The TP intensity required for a π rotation can be extracted from these fits as $I_\pi = \pi/\beta$, and is shown in Fig. 4C as a function of detuning, displaying the expected linear dependence. If the expected slope of this line is estimated from Eq. 1 with reasonable parameters, we find a discrepancy of about a factor of 10 from the measured value, which may be due to a number of experimental uncertainties (*21*).

The data in Fig. 4A most clearly show the effects of DNP on the observed spin dynamics. In the absence of nuclear polarization, one would expect the curves in Fig. 4A to be cosinusoidal, crossing zero at an intensity half that required for a π rotation. DNP, however, which is maximal when $\phi_{tip} \approx \pi/2$, distorts this ideal cosine form, as is well described by the model (*21*). Additionally, an effect of the misalignment of the initial spin direction out of the *x*-*y* plane can be seen in the signal near I_{tip} = 0. The TP first rotates the spin into the *x*-*y* plane, increasing the signal slightly, and then rotates it past the *x*-*y* plane as I_{tip} is increased. This is confirmed by reversing the helicity of the TP so that the spin rotation is in the same direction as the misalignment, instead of

against it. [This and further control measurements are discussed in (*21*).]

Much of the deviation of the data from the model can be explained by the slow drift of experimental parameters during the measurement. In particular, the observed effects are very sensitive to the focus on the sample, because the intensities of the pump, probe, and TP all vary quadratically with the focused spot size. Additional deviations may be due to the simplistic description of the TP-induced background effects used here. For example, in the case of phonon-assisted transitions to the trion state, one would expect the type of spin-selective decoherence described in (*18*). Although there is some finite probability for the TP to excite the trion state, the control measurements described in the supporting online text show that TP-induced spin coherence is not the dominant mechanism for the spin control observed here. Further measurements of the background effects will be needed to determine their cause, with the aim of increasing the fidelity of these single spin rotations.

In principle, at most 200 single-qubit flips could be performed within the measured T_2^* of 6 ns. However, by using shorter TPs and QDs with longer spin coherence times, this technique could be extended to perform many more operations within the coherence time. A mode-locked laser producing ~100-fs TPs could potentially exceed the threshold (~10^4 operations) needed for proposed quantum error-correction schemes (*28*). Additionally, the spin manipulation demonstrated here may be used to obtain a spin echo (*29*), possibly extending the observed spin coherence time. These results represent progress toward the implementation of scalable quantum information processing in the solid state.

References and Notes

1. A. Imamoglu *et al.*, *Phys. Rev. Lett.* **83**, 4204 (1999).
2. M. Combescot, O. Betbeder-Matibet, *Solid State Commun.* **132**, 129 (2004).
3. P. Chen, C. Piermarocchi, L. J. Sham, D. Gammon, D. G. Steel, *Phys. Rev. B* **69**, 075320 (2004).
4. C. E. Pryor, M. E. Flatté, *Appl. Phys. Lett.* **88**, 233108 (2006).
5. S. E. Economou, L. J. Sham, Y. Wu, D. G. Steel, *Phys. Rev. B* **74**, 205415 (2006).
6. S. M. Clark, K.-M. C. Fu, T. D. Ladd, Y. Yamamoto, *Phys. Rev. Lett.* **99**, 040501 (2007).
7. F. H. L. Koppens *et al.*, *Nature* **442**, 766 (2006).
8. K. C. Nowack, F. H. L. Koppens, Y. V. Nazarov, L. M. K. Vandersypen, *Science* **318**, 1430 (2007).
9. C. Cohen-Tannoudji, J. Dupont-Roc, *Phys. Rev. A* **5**, 968 (1972).
10. C. Cohen-Tannoudji, S. Reynaud, *J. Phys. B* **10**, 345 (1977).
11. D. Suter, H. Klepel, J. Mlynek, *Phys. Rev. Lett.* **67**, 2001 (1991).
12. M. Combescot, R. Combescot, *Phys. Rev. Lett.* **61**, 117 (1988).
13. M. Joffre, D. Hulin, A. Migus, M. Combescot, *Phys. Rev. Lett.* **62**, 74 (1989).
14. G. Papageorgiou *et al.*, *Phys. Rev. B* **69**, 085311 (2004).
15. J. A. Gupta, R. Knobel, N. Samarth, D. D. Awschalom, *Science* **292**, 2458 (2001).
16. T. Unold, K. Mueller, C. Lienau, T. Elaesser, A. D. Wieck, *Phys. Rev. Lett.* **92**, 157401 (2004).
17. M. V. Gurudev Dutt *et al.*, *Phys. Rev. B* **74**, 125306 (2006).
18. Y. Wu *et al.*, *Phys. Rev. Lett.* **99**, 097402 (2007).
19. A. Greilich *et al.*, *Phys. Rev. B* **75**, 233301 (2007).
20. S. G. Carter, Z. Chen, S. T. Cundiff, *Phys. Rev. B* **76**, 201308 (2007).
21. Supporting material is available on *Science* Online.
22. J. Berezovsky *et al.*, *Science* **314**, 1916 (2006).
23. M. H. Mikkelsen, J. Berezovsky, N. G. Stoltz, L. A. Coldren, D. D. Awschalom, *Nat. Phys.* **3**, 770 (2007).
24. F. Meier, B. P. Zakharchenya, Eds., *Optical Orientation: Modern Problems in Condensed Matter* (North Holland, Amsterdam, 1984).
25. M. Atatüre, J. Dreiser, A. Badolato, A. Imamoglu, *Nat. Phys.* **3**, 101 (2007).
26. A. Von Lehmen, J. E. Zucker, J. P. Heritage, D. S. Chemla, *Phys. Rev. B* **35**, 6479(R) (1987).
27. D. Gammon *et al.*, *Phys. Rev. Lett.* **86**, 5176 (2001).
28. D. D. Awschalom, D. Loss, N. Samarth, Eds., *Semiconductor Spintronics and Quantum Computation* (Springer-Verlag, Berlin, 2002).
29. M. Rosatzin, D. Suter, J. Mlynek, *Phys. Rev. A* **42**, 1839(R) (1990).

30. We acknowledge support from NSF and the Air Force Office of Scientific Research.

Supporting Online Material

www.sciencemag.org/cgi/content/full/320/5874/349/DC1
Materials and Methods
SOM Text
Figs. S1 and S2
References

15 October 2007; accepted 26 February 2008
10.1126/science.1154798

Coherent Dynamics of a Single Spin Interacting with an Adjustable Spin Bath

R. Hanson,[1]*† V. V. Dobrovitski,[2] A. E. Feiguin,[1] O. Gywat,[1] D. D. Awschalom[1]

Phase coherence is a fundamental concept in quantum mechanics. Understanding the loss of coherence is paramount for future quantum information processing. We studied the coherent dynamics of a single central spin (a nitrogen-vacancy center) coupled to a bath of spins (nitrogen impurities) in diamond. Our experiments show that both the internal interactions of the bath and the coupling between the central spin and the bath can be tuned in situ, allowing access to regimes with surprisingly different behavior. The observed dynamics are well explained by analytics and numerical simulations, leading to valuable insight into the loss of coherence in spin systems. These measurements demonstrate that spins in diamond provide an excellent test bed for models and protocols in quantum information.

Quantum systems interact with their environment, resulting in a loss of initial coherence over time (*1*). Such system-bath interactions are studied extensively in a few canonical examples such as the spin-boson model (*2*) and the central spin model. In the latter, the coherence of a single spin (the central spin) in contact with a bath of spins is investigated (*3*–*11*). Study of the central spin problem may shed light on the emergence of the classical world from a collection of interacting quantum systems (*1*). Moreover, understanding spin-bath interactions is crucial for using spins in solids for quantum information processing (*12*–*14*), in which the efficient isolation of single quantum systems from their environment is required.

Studies in the field of nuclear magnetic resonance (NMR) and electron spin resonance have yielded detailed information about magnetic interactions in ensembles of spins (*15*). Recently, it has become possible to detect and coherently control individual spins (*16*, *17*), allowing studies of the central spin model on truly single spins and possible applications in high-resolution magnetometry (*18*). We report here on a detailed study of the coherent dynamics of a single spin of a nitrogen-vacancy (NV) center in contact with a bath of nitrogen (N) impurity spins in diamond.

NV centers are well suited for studying spin interactions: Their spin state can be optically imaged, initialized, and read out, as well as controlled with high fidelity. In ultrapure diamond, the spin coherence time reaches hundreds of microseconds, being limited only by the weak interactions with nuclear spins of carbon-13 (*19*, *20*). Therefore, the presence of nearby electron spins in diamond, even if few in number, can strongly influence the NV center spin, as the magnetic moment of an electron spin is three orders of magnitude larger than that of a nuclear spin.

In type Ib diamonds, as studied here, the magnetic environment of an NV center is dominated by N impurities (*21*), which carry an electronic spin of 1/2. These N spins are not optically active themselves but can be detected through the magnetic dipolar coupling with the NV center spin (*22*, *23*). Previously, spin pairs were studied in which the dynamics of a single NV center spin were dominated by a single nearby N spin (*19*, *24*). We studied the opposite regime, where the central spin (the NV center) is

[1]California Nanosystems Institute, University of California, Santa Barbara, CA 93106, USA. [2]Ames Laboratory and Iowa State University, Ames, IA 50011, USA.

*Present address: Kavli Institute of Nanoscience Delft, Delft University of Technology, Post Office Box 5046, 2600 GA Delft, Netherlands.

†To whom correspondence should be addressed. E-mail: r.hanson@tudelft.nl